INTERNATIONAL JOURNAL FOR NUMERICAL METHODS IN FLUIDS, VOL. 10, 811–825 (1990)

BOUNDARY ELEMENT CALCULATION OF SHALLOW WATER WAVES

N. KANEKO AND N. UTAGAWA

Engineering Research Institute, Sato kogyo Co., Ltd., 47-3 Sanda, Atsugi, Kanagawa 243-02, Japan

AND

M. KAWAHARA

Department of Civil Engineering, Chuo University, 1-13-27 Kasuga, Bunkyo, Tokyo 112, Japan

SUMMARY

A boundary element method is proposed for studying periodic shallow water problems. The numerical model is based on the shallow water equation. The key feature of this method is that the boundary integral equations are derived using the weighted residual method and the fundamental solutions for shallow water wave problems are obtained by solving the simultaneous singular equations. The accuracy of this method is studied for the wave reflection problem in a rectangular tank. As a result of this test, it has been shown that the number of element divisions and the distribution of nodes are significant to the accuracy. For numerical examples of external problems, the wave diffraction problems due to single cylindrical, double cylindrical and plate obstructions are analysed and compared with the exact and other numerical solutions. Relatively accurate solutions are obtained.

KEY WORDS Boundary element method Shallow water equation Wave reflection Wave diffraction

1. INTRODUCTION

When constructing artificial islands or reclamation areas along the ocean side, it is important and necessary to predict the water quality in advance and to assess the damage of disasters such as tsunamis and storm surges. Numerical simulation is one of the most powerful techniques for such assessments, because it is advantageous for studies that have many parameters and uncertain variables included.

Numerical techniques for shallow water waves have already been applied to problems such as tidal waves, tsunamis, storm surges and secondary waves in a harbour. Finite element and finite difference methods have been widely used for solving the shallow water equations.[1–5] These methods involve some problems to be solved. To improve the accuracy of simulations, very fine meshes or grids are required. Therefore the CPU time becomes very long and a large memory capacity is necessary. The other problem is the treatment of the open boundary. It is evident that these techniques have limitations and must employ a large domain to include the effect of the infinite boundary condition approximately. For the purpose of representing the effect of the infinite region, several techniques to deal with the boundary of the domain have been proposed.[6–8]

0271–2091/90/070811–15$07.50

Received February 1989
Revised September 1989

On the other hand, numerical methods based on the boundary integral equation (boundary element method) have been developed for solving ocean wave problems. These methods have some merits for solving ocean wave problems. Firstly, it is easy to satisfy the radiation condition in the infinite region. Accordingly, this method has been applied to ocean wave problems which involve the open boundary.[9] Secondly, it is simple to treat the free surface boundary because of discretizing only on the boundary. Therefore non-linear waves such as solitary and cnoidal waves have been simulated by Nakayama[10] and Ohyama.[11] The response analysis of a floating body under regular waves has been performed for the above reasons.[12]

In this paper we propose a boundary element method for solving the shallow water wave equations. The shallow water equations are derived from the three-dimensional Navier–Stokes equations by integrating over the depth and assuming hydrostatic pressure. There are three approaches for solving such time-dependent problems: (1) a method in the frequency domain; (2) a method using time-dependent fundamental solutions; (3) a coupled boundary element–finite difference method.[13] The first approach is employed in this paper from the viewpoint of application to open boundary problems. This approach does not require domain integrals and it is easy to satisfy the radiation condition. The boundary integral equations are formulated using the weighted residual method. The fundamental solutions are obtained by solving simultaneous singular differential equations by means of Fourier transformation. A formulation dealing with incident waves from the infinite region is put forward. Several numerical tests are presented: one concerns an internal problem, the wave reflection in a rectangular tank; the other involves an external problem, the wave diffraction due to cylindrical and plate obstructions. The performance characteristics of the proposed method are discussed in the light of the numerical tests.

2. BASIC EQUATIONS

Basic equations which satisfy the following assumptions are used:

(a) linear shallow water wave theory (the convective term, the Coriolis force and the frictional force are all neglected.)
(b) sinusoidal waves
(c) water depth is constant throughout the region
(d) water elevation is much smaller than the depth
(e) turbulence can be expressed by the constant eddy viscosity.

Those phenomena can be described by the momentum and continuity equations in the following manner. Let u_i be the horizontal velocity, ζ the water elevation and t_i the traction; u_i, ζ and t_i are the solutions of

momentum equation
$$\frac{\partial u_i}{\partial t} - \tau_{ij,j} = 0 \quad \text{in the region } \Omega, \tag{1}$$
$$\tau_{ij} = -g\zeta\delta_{ij} + \nu(u_{i,j} + u_{j,i}),$$

continuity equation
$$\frac{\partial \zeta}{\partial t} + Hu_{i,i} = 0 \quad \text{in the region } \Omega, \tag{2}$$

boundary conditions
$$u_i = \hat{u}_i, \quad t_i = \hat{t}_i = \tau_{ij} n_j \quad \text{on the boundary } \Gamma, \tag{3}$$

where H is the water depth, g is the gravitational acceleration, δ_{ij} is the Kronecker delta, ν is the eddy viscosity, n_j are components of unit normals to the boundary and $\hat{}$ denotes prescribed values on the boundary.

For the sinusoidal wave the unknown variables u_i and ζ can be expressed in terms of time and space co-ordinates by the following equation:

$$u_i = \bar{u}_i e^{i\omega t}, \qquad \zeta = \bar{\zeta} e^{i\omega t}, \tag{4}$$

where ω is the angular frequency and the amplitudes $\bar{u}_i$ and $\bar{\zeta}$ are defined as a function of location. The following equations can be obtained by substituting equation (4) into equations (1) and (2):

$$i\omega \bar{u}_i - \bar{\tau}_{ij,j} = 0, \tag{5}$$

$$i\omega \bar{\zeta} + H\bar{u}_{i,i} = 0. \tag{6}$$

Hereafter, the overbars are neglected for simplicity of expression.

3. BOUNDARY INTEGRAL EQUATIONS

Two different boundary integral equations are devised to calculate the values of velocity and water elevation. These equations are formulated using the weighted residual method. Fundamental solutions are obtained by solving the simultaneous singular differential equations by means of Fourier transformation.

3.1. Boundary integral equation for velocity

The following equation is obtained from equations (5) and (6) after some simple mathematical manipulation:

$$\int_\Omega [\zeta_k^* g(i\omega\zeta + Hu_{i,i}) - u_{ki}^* H(i\omega u_i - \tau_{ij,j})]\, d\Omega = 0, \tag{7}$$

where u_{ki}^* and ζ_k^* are the fundamental solutions, which show the velocity and water elevation at the observation point in the i-direction corresponding to a unit velocity acting in the k-direction at the source point. Green's theorem leads to the following equation:

$$\int_\Omega g\zeta(i\omega\zeta_k^* + Hu_{ki,i}^*)\, d\Omega - \int_\Omega Hu_i\{i\omega u_{ki}^* - [-g\zeta_k^* \delta_{ij} + \nu(u_{ki,j}^* + u_{kj,i}^*)]_{,j}\}\, d\Omega$$
$$- \int_\Gamma HT_{ki}^* u_i\, d\Gamma + \int_\Gamma Hu_{ki}^* t_i\, d\Gamma = 0, \tag{8}$$

where

$$T_{ki}^* = [-g\zeta_k^* \delta_{ij} + \nu(u_{ki,j}^* + u_{kj,i}^*)]n_j.$$

Let the fundamental solutions u_{ki}^* and ζ_k^* satisfy the following equations, where $\delta(x)$ denotes the Dirac delta function:

$$i\omega u_{ki}^* - [-g\zeta_k^* \delta_{ij} + \nu(u_{ki,j}^* + u_{kj,i}^*)]_{,j} + \delta_{ki}\delta(x)\delta(y) = 0, \tag{9}$$

$$i\omega\zeta_k^* + Hu_{ki,i}^* = 0. \tag{10}$$

Substituting equations (9) and (10) into equation (8) and using the fact that the first term is zero and the second term is Hu_i because of the character of the Dirac delta function, the boundary integral equation for velocity is obtained as follows:

$$u_k - \int_\Gamma T_{ki}^* u_i\, d\Gamma + \int_\Gamma u_{ki}^* t_i\, d\Gamma = 0. \tag{11}$$

The fundamental solutions u_{ki}^* and ζ_k^* are derived by solving the simultaneous singular differential equations (9) and (10) by means of Fourier transformation:

$$u_{ki}^* = \psi(R)\delta_{ki} + \chi(R)\frac{dR}{dx_k}\frac{dR}{dx_i}, \tag{12}$$

$$\zeta_k^* = \frac{iH\omega}{4C_1^3} H_1^{(2)}\left(\frac{\omega}{C_1}R\right)\frac{dR}{dx_k}, \tag{13}$$

where

$$\psi(R) = \frac{\omega}{4C_2^2}\left[H_0^{(2)}\left(\frac{\omega}{C_2}R\right) + \frac{C_2^2}{\omega R C_1} H_1^{(2)}\left(\frac{\omega}{C_1}R\right) - \frac{C_2}{\omega R} H_1^{(2)}\left(\frac{\omega}{C_2}R\right)\right],$$

$$\chi(R) = -\frac{\omega}{4C_2^2}\left(H_2^{(2)}\left(\frac{\omega}{C_2}R\right) - \frac{C_2^2}{C_1^2} H_2^{(2)}\left(\frac{\omega}{C_1}R\right)\right].$$

Here $H_n^{(2)}$ is the nth-order Hankel function of the second kind, R is the distance between source and observation points, $C_1 = (gH + 2i\omega\nu)^{1/2}$ and $C_2 = (i\omega\nu)^{1/2}$.

Boundary integral equation on the boundary is obtained by integrating around the point on the boundary and by the process $\varepsilon \to 0$. In view of the singularity of the fundamental solution on the boundary, the boundary integral equation (11) is transformed as follows;

$$C_{pk}^{(p)} u_p - \int_\Gamma T_{ki}^* u_i \, d\Gamma + \int_\Gamma u_{ki}^* t_i \, d\Gamma = 0, \tag{14}$$

where

$$C_{11}^{(p)} = \frac{1}{2\pi}\left(2\pi + (\beta_1 - \beta_2) + \frac{1}{2}\frac{C_1^2 - C_2^2}{C_1^2}(\sin 2\beta_1 - \sin 2\beta_2)\right),$$

$$C_{12}^{(p)} = C_{21}^{(p)} = \frac{1}{2\pi}\frac{C_1^2 - C_2^2}{C_1^2}(\sin^2\beta_1 - \sin^2\beta_2),$$

$$C_{22}^{(p)} = \frac{1}{2\pi}\left(2\pi + (\beta_1 - \beta_2) - \frac{1}{2}\frac{C_1^2 - C_2^2}{C_1^2}(\sin 2\beta_1 - \sin 2\beta_2)\right).$$

The angles β_1 and β_2 are defined in Figure 1.

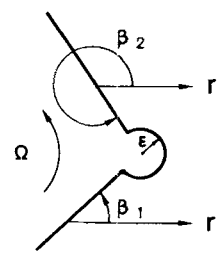

Figure 1. Definition of angles

3.2. Boundary integral equation for water elevation

The following equation is obtained from equations (5) and (6) after some simple mathematical manipulation:

$$\int_\Omega [\tilde{\zeta}^* g(\mathrm{i}\omega\zeta + Hu_{i,i}) - \tilde{u}_i^* H(\mathrm{i}\omega u_i - \tau_{ij,j})]\,\mathrm{d}\Omega = 0, \tag{15}$$

where $\tilde{u}_i^*$ and $\tilde{\zeta}^*$ show the velocity and water elevation at the observation point in the i-direction corresponding to a unit water elevation at the source point. Green's theorem leads to the following equation:

$$\int_\Omega g\zeta(\mathrm{i}\omega\tilde{\zeta}^* + H\tilde{u}_{i,i}^*)\,\mathrm{d}\Omega - \int_\Omega Hu_i\{\mathrm{i}\omega\tilde{u}_i^* - [-g\tilde{\zeta}^*\delta_{ij} + \nu(\tilde{u}_{i,j}^* + \tilde{u}_{j,i}^*)]_{,j}\}\,\mathrm{d}\Omega$$
$$- \int_\Gamma H\tilde{t}_i^* u_i\,\mathrm{d}\Gamma + \int_\Gamma H\tilde{u}_i^* t_i\,\mathrm{d}\Gamma = 0. \tag{16}$$

Let the fundamental solutions $\tilde{u}_i^*$ and $\tilde{\zeta}^*$ satisfy the following equations:

$$\mathrm{i}\omega\tilde{u}_i^* - [-g\tilde{\zeta}^*\delta_{ij} + \nu(\tilde{u}_{i,j}^* + \tilde{u}_{j,i}^*)]_{,j} = 0, \tag{17}$$

$$\mathrm{i}\omega\tilde{\zeta}^* + H\tilde{u}_{i,i}^* + \delta(x)\delta(y) = 0. \tag{18}$$

The boundary integral equation for water elevation is obtained by substituting equations (17) and (18) into equation (16) as

$$\zeta + \int_\Gamma \frac{H}{g}\tilde{t}_i^* u_i\,\mathrm{d}\Gamma - \int_\Gamma \frac{H}{g}\tilde{u}_i^* t_i\,\mathrm{d}\Gamma = 0. \tag{19}$$

The fundamental solutions $\tilde{u}_i^*$ and $\tilde{\zeta}^*$ are obtained by solving the simultaneous singular differential equations (17) and (18) by means of Fourier transformation:

$$u_i^* = \frac{\mathrm{i}g\omega}{4C_1^3} H_1^{(2)}\left(\frac{\omega}{C_1}R\right)\frac{\mathrm{d}R}{\mathrm{d}x_i}, \tag{20}$$

$$\tilde{\zeta}^* = \frac{\omega}{4C_1^4}(2C_2^2 - C_1^2)H_0^{(2)}\left(\frac{\omega}{C_2}R\right). \tag{21}$$

3.3. Boundary integral equations with consideration of incident waves

The velocity is assumed to be the sum of the incident velocity $u_i^{(\mathrm{I})}$ and the scattered velocity $u_i^{(\mathrm{S})}$:

$$u_i = u_i^{(\mathrm{I})} + u_i^{(\mathrm{S})}. \tag{22}$$

The boundary integral equation (11) is decomposed into boundary integral terms both for infinite regions and around a body. Equation (22) is substituted into the boundary integral term for infinite regions to give

$$u_k - \int_\Gamma T_{ki}^* u_i\,\mathrm{d}\Gamma + \int_\Gamma u_{ki}^* t_i\,\mathrm{d}\Gamma - \int_{\Gamma_\infty} T_{ki}^* u_i^{(\mathrm{I})}\,\mathrm{d}\Gamma + \int_{\Gamma_\infty} u_{ki}^* t_i^{(\mathrm{I})}\,\mathrm{d}\Gamma - \int_{\Gamma_\infty} T_{ki}^* u_i^{(\mathrm{S})}\,\mathrm{d}\Gamma + \int_{\Gamma_\infty} u_{ki}^* t_i^{(\mathrm{S})}\,\mathrm{d}\Gamma = 0. \tag{23}$$

The incident velocity $u_i^{(\mathrm{I})}$ is the solution of equation (11), which is expressed as

$$u_k^{(\mathrm{I})} - \int_\Gamma T_{ki}^* u_i^{(\mathrm{I})}\,\mathrm{d}\Gamma + \int_\Gamma u_{ki}^* t_i^{(\mathrm{I})}\,\mathrm{d}\Gamma - \int_{\Gamma_\infty} T_{ki}^* u_i^{(\mathrm{I})}\,\mathrm{d}\Gamma + \int_{\Gamma_\infty} u_{ki}^* t_i^{(\mathrm{I})}\,\mathrm{d}\Gamma = 0. \tag{24}$$

The boundary integral term around a body is equal to zero by Cauchy's theorem:

$$u_k^{(\mathrm{I})} - \int_{\Gamma_\infty} T_{ki}^* u_i^{(\mathrm{I})} \, \mathrm{d}\Gamma + \int_{\Gamma_\infty} u_{ki}^* t_i^{(\mathrm{I})} \, \mathrm{d}\Gamma = 0. \tag{25}$$

The sixth and seventh terms in equation (23) are equal to zero by the radiation condition. The boundary integral equation for velocity with consideration of incident waves is obtained by substituting equation (25) into the fourth and fifth terms:

$$u_k - \int_\Gamma T_{ki}^* u_i \, \mathrm{d}\Gamma + \int_\Gamma u_{ki}^* t_i \, \mathrm{d}\Gamma - u_k^{(\mathrm{I})} = 0. \tag{26}$$

Here the incident velocity $u_i^{(\mathrm{I})}$ can be expressed by the potentials φ and ψ which are the solutions of the basic equations, because $u_i^{(\mathrm{I})}$ is a regular function:

$$u_z^{(\mathrm{I})} = \frac{\partial \varphi}{\partial x} - \frac{\partial \psi}{\partial y}, \tag{27}$$

$$u_y^{(\mathrm{I})} = \frac{\partial \varphi}{\partial y} + \frac{\partial \psi}{\partial x}, \tag{28}$$

where

$$\varphi = A \exp\left(-\frac{\mathrm{i}\omega}{C_1} (x \cos\theta + y \sin\theta) \right), \qquad \psi = B \exp\left(-\frac{\mathrm{i}\omega}{C_2} (x \cos\theta + y \sin\theta) \right). \tag{29}$$

The water elevation is expressed by the potential as follows:

$$\zeta = \frac{H}{\mathrm{i}\omega} u_{i,i} = \frac{H\omega}{\mathrm{i}C_1^2} \varphi, \tag{30}$$

Here the water elevation due to the velocity of incident waves can be expressed by equation (30). The boundary integral equation for water elevation with consideration of incident waves is obtained by adding equations (30) and (19) as follows:

$$\zeta = \int_\Gamma \frac{H}{g} \tilde{u}_i^* t_i \, \mathrm{d}\Gamma - \int_\Gamma \frac{H}{g} \tilde{t}_i^* u_i \, \mathrm{d}\Gamma + \frac{H\omega}{\mathrm{i}C_1^2} \varphi. \tag{31}$$

4. BOUNDARY ELEMENT METHOD

It is assumed that velocity u_i and traction t_i are linearly varying. The boundary is split into a number of linear elements. The values of u_i and t_i at an arbitrary point inside an element can be computed by employing the nodal values and linear interpolation functions such that

$$u_i = \varphi_\alpha u_{\alpha i}, \qquad t_i = \varphi_\alpha t_{\alpha i}. \tag{32}$$

The following boundary element equations are obtained by substituting equation (32) into the boundary integral equations (14) and (19):

$$C_{ki}^{(p)} u_i - \sum_{k=1}^{n} \sum_{j=1}^{n} \int_{\Gamma_j} T_{ki}^* \varphi_\alpha \, \mathrm{d}\Gamma \{u_{\alpha i}\} + \sum_{k=1}^{n} \sum_{j=1}^{n} \int_{\Gamma_j} u_{ki}^* \varphi_\alpha \, \mathrm{d}\Gamma \{t_{\alpha i}\} = 0, \tag{33}$$

$$\zeta + \sum_{j=1}^{n} \int_{\Gamma_j} \frac{H}{g} \tilde{t}_i^* \varphi_\alpha \, \mathrm{d}\Gamma \{u_{\alpha i}\} - \sum_{j=1}^{n} \int_{\Gamma_j} \frac{H}{g} \tilde{u}_i^* \varphi_\alpha \, \mathrm{d}\Gamma \{t_{\alpha i}\} = 0, \tag{34}$$

when n is the number of linear boundary elements. The following equations are derived by assembling equations (33) and (34) for all nodal points to give,

$$\mathbf{Hu} = \mathbf{Gt}, \tag{35}$$

$$\zeta = \tilde{\mathbf{H}}\mathbf{u} + \tilde{\mathbf{G}}\mathbf{t}. \tag{36}$$

The unknown variables u_i and t_i on the boundary are calculated using equation (35). The velocity and water elevation in the domain are obtained by substituting the values u_i and t_i on the boundary into equations (35) and (36). The non-diagonal coefficients in the matrices **H** and **G** are integrated using Gaussian quadrature. Because the diagonal coefficients contain integrals with a strong singularity in the boundary integral equation on the boundary, integration is performed using series expansions of Hankel functions and the segment length h tends to zero.

5. NUMERICAL TEST CASES

Several numerical examples are carried out to validate the present method. The integral problems are calculated to assess the accuracy of this method. The external problems are calculated to investigate the possibility of application to the open boundary problem.

5.1. Wave reflection problem in a rectangular tank

The accuracy of the method is assessed by numerical experiments. The influence of different frequencies and viscosities has been studied. To improve the accuracy, discretization of boundary elements and different kinds of distributions of corner nodes have been tested.

The model given in Figure 2 has been tested for the prescribed values shown in Table I for frequency and viscosity. Sinusoidal waves with maximum velocity whose amplitude is unity are

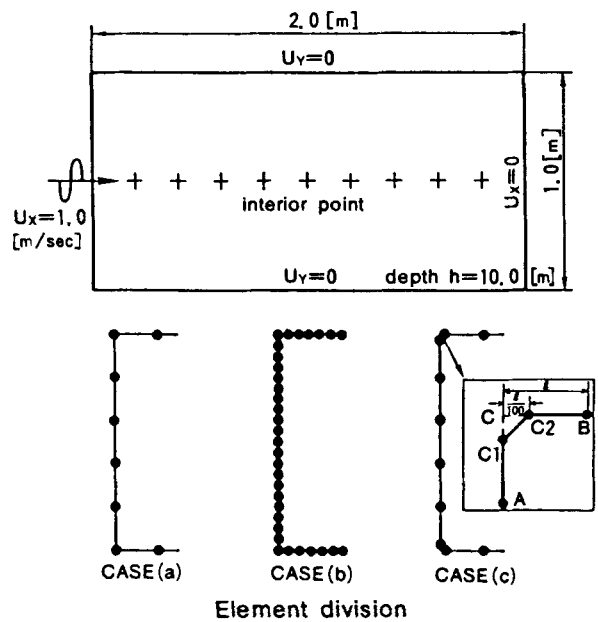

Figure 2. Test model for wave reflection problem in a rectangular tank

Table I. Test parameters

Angular frequency (rad s^{-1})	0·314, 3·14, 31·4
Eddy viscosity (m^2 s^{-1})	0·1, 1·0, 10·0
Water depth (m)	10·0
Gravitational acceleration (m s^{-2})	9·81

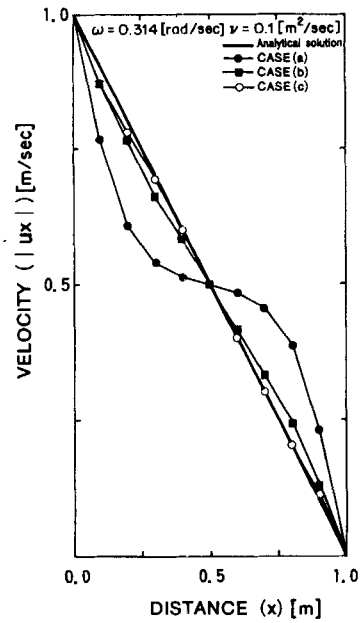

Figure 3. Comparison of velocity distribution with analytical solution ($\omega = 0{\cdot}314$, $\nu = 0{\cdot}1$)

applied on the left side wall. This case can be considered as a one-dimensional problem. For the sake of comparison, equations (5) and (6) are solved analytically for this particular problem. Therefore it becomes possible for this problem to compare the numerical result with the analytical solution at the nine interior points represented in Figure 2. The three cases of different divisions of boundary elements are illustrated in Figure 2. The numerical results for velocity for $\nu = 0{\cdot}1$ and $\omega = 0{\cdot}314$ are given in Figure 3. This figure shows that the result by using the boundary element division of Case (c) is in good agreement with the analytical solution.

The accuracy of the method is discussed for each type of division. The error is estimated by the average of the error at the nine interior points.

Case (a): Coarse boundary element division. For the first case the boundary is divided into 30 elements and the boundary conditions for the corner $U_x = U_y = 0$ are used. The computed errors for velocity are shown in Table II. The error for the high-viscosity case is less than 1%. On the other hand, the error is considerably higher in the case of low viscosity, e.g. for $\nu = 0{\cdot}1$ and $\omega = 31{\cdot}4$ the error becomes 49%. To test the influence of frequency, the error for velocity is plotted against the logarithm of ω^* in Figure 4, where the non-dimensional frequency ω^* is defined as the ratio of

Table II. Estimated error of Case (a)

Eddy viscosity ($m^2 s^{-1}$)	Angular frequency (rad s^{-1})		
	31·4159	3·14159	0·314159
0·1	59·92[a]	94·58	132·97
	49·13[b]	22·35	42·02
1·0	3·72	1·87	44·96
	2·33	0·49	13·37
10·0	0·23	0·29	0·45
	0·14	0·06	0·15

[a] Maximum (%).
[b] Average (%).

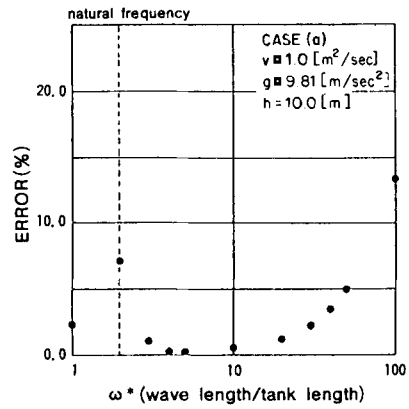

Figure 4. Plot of error versus frequency

wave length to tank length. Figure 4 indicates that the error is appreciable for high ω^*. It is noticeable that the order of error at the natural period is remarkably high.

Case (b): Fine boundary element division. In order to improve the accuracy, the boundary is divided into 120 elements. The boundary conditions for the corner are the same as in Case (a). The computed errors for velocity are shown in Table III. The average error of all cases is 2·06% for velocity, but the error at low viscosity is still high. The CPU time is about 24 times as long as that for Case (a).

Case (c): Double-corner-node procedure. It is observed that the error close to the corner is high in the case of both low viscosity and long period. Therefore a double-grid procedure at the corner of the boundary is applied to improve the accuracy. The number of elements is the same as in Case (a). The double-corner-node procedure is illustrated in Figure 2. The corner C is represented by two nodes C1 and C2 which are chosen at points infinitely close to the corner C and located on the boundaries AC and BC respectively. It should be noted that C1 is given to express the condition associated with the boundary AC, whereas C2 is given the condition on the boundary

Table III. Estated error of Case (b)

Eddy viscosity ($m^2 s^{-1}$)	Angular frequency ($rad\,s^{-1}$)		
	31·4159	3·14159	0·314159
0·1	10·26 8·86	2·71 0·45	29·67 8·97
1·0	0·24 0·15	0·19 0·04	0·30 0·11
10·0	0·03 0·01	0·10 0·01	0·10 0·02

Table IV. Estimated error of Case (c)

Eddy viscosity ($m^2 s^{-1}$)	Angular frequency ($rad\,s^{-1}$)		
	31·4159	3·14159	0·314159
0·1	10·51 8·12	2·12 1·01	11·49 2·68
1·0	2·91 2·14	2·34 1·13	2·42 1·12
10·0	6·92 5·53	3·77 2·84	2·34 1·06

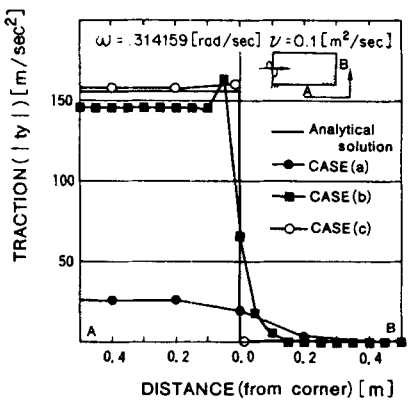

Figure 5. Traction near the corner

BC. The computed errors are shown in Table IV. Although the element division is the same as in Case (a), the accuracy is remarkably improved. In particular, at low viscosity the average error is 3·94% for velocity, which is about one-tenth of that in Case (a). However, at high viscosity the error becomes slightly higher than in Case (a). The reason for the improved accuracy using the double-corner-node procedure can be discussed as follows. The distribution of traction close to the corner is shown in Figure 5. For Case (c) the exact solution of the traction is distributed as a

step function close to the corner and has two values at the corner node. In Case (a) and Case (b), using the boundary conditions for the corner $U_x = U_y = 0$, the variables such as velocity and traction at the corner node have only one value. Therefore in the case of an analysis which has an unsmooth boundary, the error increases with these boundary conditions. In particular, the error increases because the discrepancy becomes wider at low viscosity. In these cases it is interesting to note that the accuracy of the numerical solution is improved considerably by adopting the proposed double-corner-node procedure. The CPU time is almost the same as in Case (a).

5.2. *Wave diffraction problem*

The present method is applied to three kinds of diffraction problems due to single cylindrical, double cylindrical and plate obstructions. These numerical results are compared with the exact solution and with numerical solutions by other methods.

(*a*) *Single cylindrical obstruction.* The diffraction problem due to a single cylindrical obstruction is analysed. The model is shown in Figure 6. Numerical examples are calculated with respect to eddy viscosities of 0·1, 1·0 and 10·0. The incident wave is such that the amplitude of the water elevation at the centre of the cylindrical obstruction becomes 1·0. The boundary around the cylindrical obstruction is divided into 60 elements. The length of the boundary corresponds to the length of the wave. The numerical solutions are compared with the theoretical solutions for a perfect fluid.[14] The four contours of the absolute amplitude of the water elevation are compared in Figure 7. It is observed that the numerical solutions are similar to the theoretical solutions. The distributions of the water elevation surrounding the obstruction are compared in Figure 8. It is

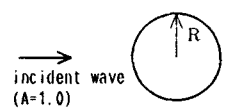

Figure 6. Test model for wave diffraction problem (a)

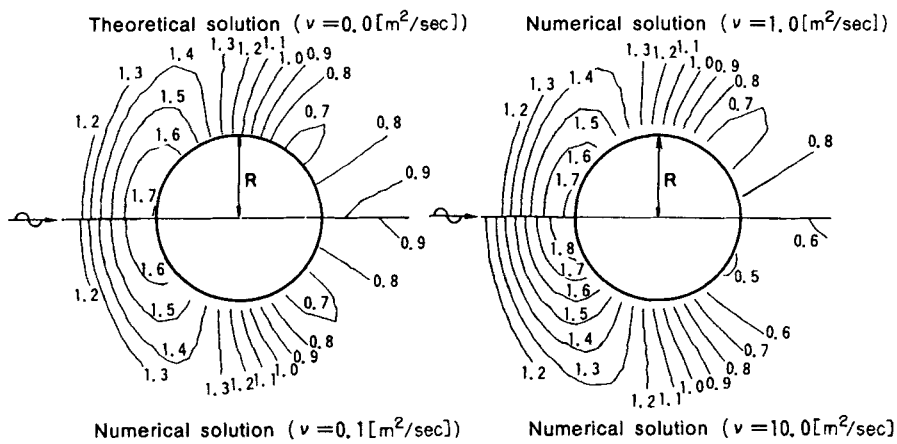

Figure 7. Contours of absolute amplitude of water elevation ($KR = 1{\cdot}0$)

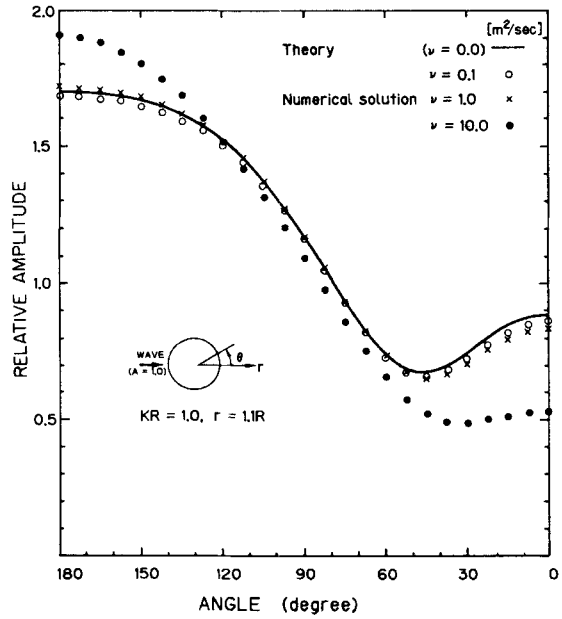

Figure 8. Comparison between numerical and theoretical wave amplitude surrounding the obstruction

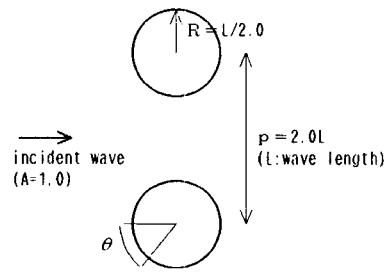

Figure 9. Test model for wave diffraction problem (b)

shown that the result by this method is close to the theoretical solution as the eddy viscosity becomes smaller value.

(*b*) *Double cylindrical obstruction.* The diffraction problem due to a double cylindrical obstruction is analysed. The model is shown in Figure 9. The boundary around each cylindrical obstruction is divided into 60 elements. The diameter corresponds to the length of the wave. The distribution of the water elevation surrounding the obstruction on the underside is compared with the numerical solution by Kashiyama[15] in Figure 10. It is observed that our result is similar to the numerical solution. It is concluded that this method is applicable to the wave diffraction problem due to one or many obstructions.

(*c*) *Plate obstruction.* The diffraction problem due to plate obstruction is analysed. The model is shown in Figure 11. The boundary around the plate obstruction is divided into 38 elements.

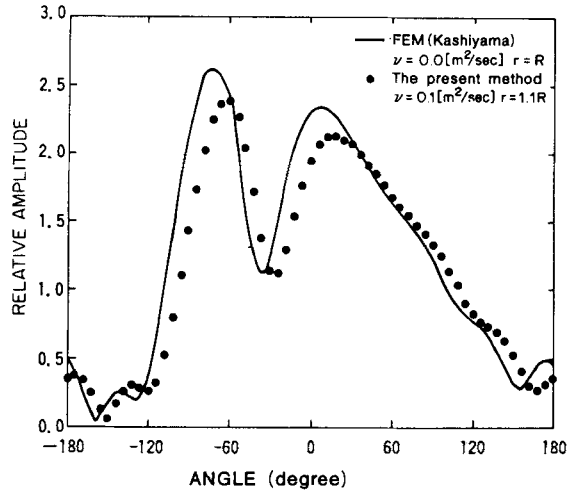

Figure 10. Distribution of water elevation surrounding the obstruction on the underside

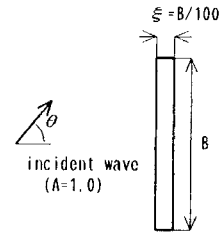

Figure 11. Test model for wave diffraction problem (c)

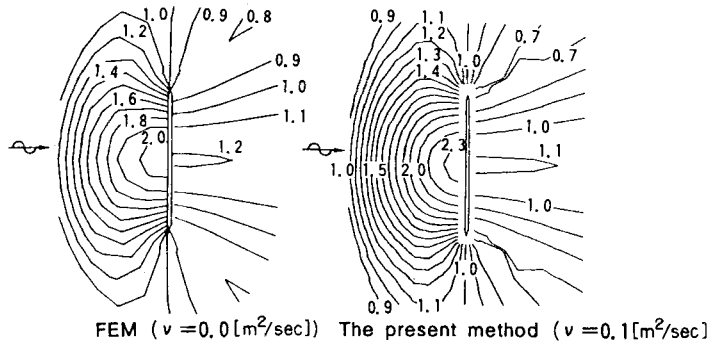

Figure 12. Comparison between results of this method and Reference 16 ($\theta = 0°$)

Numerical examples are calculated with respect to incident waves with angles of attack of 0° and 45° against the plate obstruction. The incident wave is such that the amplitude of the water elevation at the centre of plate obstruction is specified. The length of the incident wave is three times as long as the length of the long side of the plate. The results of this method are shown in Figures 12 and 13. They are compared with the numerical solution by Kawahara and

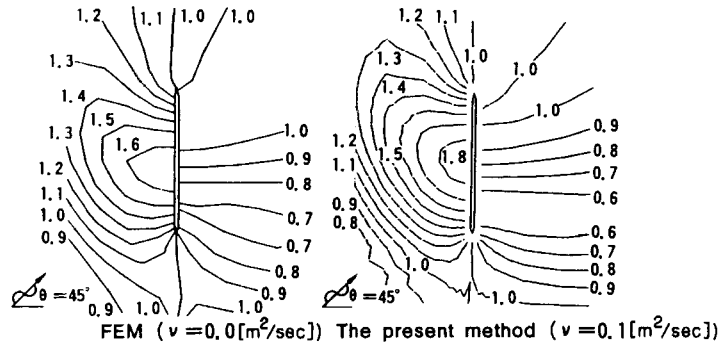

Figure 13. Comparison between results of this method and Reference 16 ($\theta = 45°$)

Kashiyama.[16] It is observed that the distribution of the water elevation by our method is similar to that of the numerical solution.

6. CONCLUSIONS

A boundary element method for solving periodic shallow water wave problems is proposed in this paper. The boundary integral equations are formulated using the weighted residual method. The fundamental solutions are obtained by solving simultaneous singular differential equations by means of Fourier transformation. Incident waves from the infinite region are considered in this method.

Several numerical tests are performed to show the validity of the method. For the first numerical example of an internal problem, the wave reflection problem in a rectangular tank is analysed. The accuracy of the method is tested by comparison with the analytical solution. As a result of this test, it is found that the number of element divisions and the distribution of the nodes are significant to the accuracy. For numerical examples of external problems, the wave diffraction problems due to single cylindrical, double cylindrical and plate obstructions are analysed. Relatively accurate solutions are obtained in these problems. It can be concluded that this method is applicable to practical shallow water wave problems with consideration of the open boundary condition.

REFERENCES

1. M. Kawahara, M. Kobayashi and K. Nakata, 'Multiple level finite element analysis and its application to tidal current flow in Tokyo bay', *Appl. Math. Modelling*, **7**, 197–211 (1983).
2. J. Peraire, O. C. Zienkiewicz and K. Morgan, 'Shallow water problems: a general explicit formulation', *Int. j. numer. methods eng.* **22**, 547–574 (1986).
3. M. Kawahara, H. Hirano, K. Tsubota and K. Inagaki, 'Selective lumping finite element method for shallow water flow', *Int. j. numer. methods fluids*, **2**, 89–112 (1982).
4. H. Kawahara and K. Hasagawa, 'Periodic Galerkin finite element method of tidal flow', *Int. j. numer. methods eng.*, **12**, 115–127 (1978).
5. M. Kawahara, N. Takeuchi and T. Yoshida, 'Two step explicit finite element method for tsunami wave propagation analysis', *Int. j. numer. methods eng.*, **12**, 331–351, 1978.
6. P. Bettess and O. C. Zienkiewicz, 'Diffraction and refraction of surface waves using finite and infinite elements', *Int. j. numer. methods eng.*, **11**, 1271–1290 (1977).
7. O. C. Zienkiewicz, D. W. Kelly and P. Bettess, 'The coupling of the finite element and boundary solution procedures', *Int. j. numer. methods eng.*, **11**, 355–375 (1977).
8. K. Bando, P. Bettess and C. Emson, 'The effectiveness of dumpers for the analysis of exterior scalar diffraction cylinders and ellipsoids', *Int. j. numer. methods fluids*, **4**(7), 599–617 (1984).

9. M. C. Au and C. A. Brebbia, 'Diffraction of water waves by vertical cylinders using boundary elements', *Appl. Math. Modelling*, **7,** 106–114 (1983).
10. T. Nakayama, 'Boundary element analysis of nonlinear water wave problems', *Int. j. numer. methods eng.*, **19,** 953–970 (1983).
11. T. Ohyama, 'A boundary element analysis for cnoidal wave run-up', *Proc. JSCE*, **381/7,** 189–198 (1987), (in Japanese).
12. T. Kiyokawa, T. Ohyama and H. Kobayashi, 'A Green's function method applied for response analysis of floating body of arbitary shape under regular waves', *Proc. JSCE*, **332/4,** 55–65 (1983), (in Japanese).
13. N. Utagawa, N. Kanako and M. Kawahara, 'Boundary element method for shallow water flow equation', *Proc. Int. Conf. on Computational Mechanics*, XI.143–XI.148, 1986.
14. R. C. MaCamy and R. A. Fuchs, 'Wave force on a file; a diffraction theory', *Tech. Memo, 69*, U.S. Army Board, U.S. Army Corps of Engineering, 1954.
15. K. Kashiyama, 'Basic studies on linear water wave problems in computational mechanics', *Ph.D. Thesis* of Chuo Univ., 1987.
16. M. Kawahara and K. Kashiyama, 'Boundary type finite element for surface wave motion based trigonometric function interpolation', *Int. j. numer. methods eng.*, **21,** 1833–1852 (1985).